Spectroscopic evidence for Davydov-like solitons in acetanilide

G. Careri, U. Buontempo, and F. Galluzzi
Department of Physics, University of Rome, I-00185 Rome, Italy

A. C. Scott
Center for Nonlinear Studies, Los Alamos National Laboratory, Los Alamos, New Mexico 87545

E. Gratton and E. Shyamsunder
Department of Physics, University of Illinois at Urbana-Champaign, Urbana, Illinois 61801
(Received 2 April 1984)

Detailed measurements of infrared absorption and Raman scattering on crystalline acetanilide [$(CH_3CONHC_6H_5)_x$] at low temperature show a new band close to the conventional amide I band. Equilibrium properties and spectroscopic data rule out explanations based on a conventional assignment, crystal defects, Fermi resonance, and upon frozen kinetics between two different subsystems. Thus we cannot account for this band using the concepts of conventional molecular spectroscopy, but a soliton model, similar to that proposed by Davydov for α-helix in protein, is in satisfactory agreement with the experimental data.

I. INTRODUCTION

Acetanilide, $(CH_3CONHC_6H_5)_x$ or ACN, is an organic solid in which two close chains of hydrogen-bonded amide groups run through the crystal. It is an interesting system because the nearly-planar amide groups display bond distances which are close to those found in polypeptides (see Fig. 1). Both synthetic and natural polypeptides are made of several chains of such hydrogen-bonded amide groups: the infinite number of parallel chains displayed by the β sheet and the three coiled chains of the α-helix being better known examples. Since the physical properties of hydrogen-bonded amide systems are very sensitive to bond distances, we expect ACN to be a useful model system in the search for new physical features of extended polypeptides and perhaps even natural proteins.

A characteristic feature of the amide group (CONH) in polypeptides is the amide I mode, mainly involving CO stretching. This mode is observed as an ir-absorption peak at about 1665 cm^{-1} in ACN and near that value in a wide variety of materials containing the amide group. Ten years ago some details of the ir and Raman spectra for ACN were reported showing that a new amide I band appears at low temperature.[1] This new band, which we shall refer to here as the *unconventional* amide I band, is red shifted from the primary band (amide I) by about 15 wave numbers to 1650 cm^{-1}. It was suggested that the unconventional band could be related to a cooperative interaction between the hydrogen-bonded proton and the first excited state of amide I, but no quantitative theory was available at that time. A reformulation of this problem has been presented in a recent note,[2] and the purpose of this paper is to present the experimental basis for our assignment of the unconventional band. The theory of our assignment is discussed in detail in the following paper,[3] but a simplified version is presented here to facilitate interpretation of the experimental results.

To appreciate the qualitative features of our theory consider that the effect of introducing localized amide I bond energy is to displace the ground states of other low-frequency vibrations. These displacements can act as a potential well to trap amide I bond energy and prevent its dispersion via dipole-dipole–interaction effects. The idea

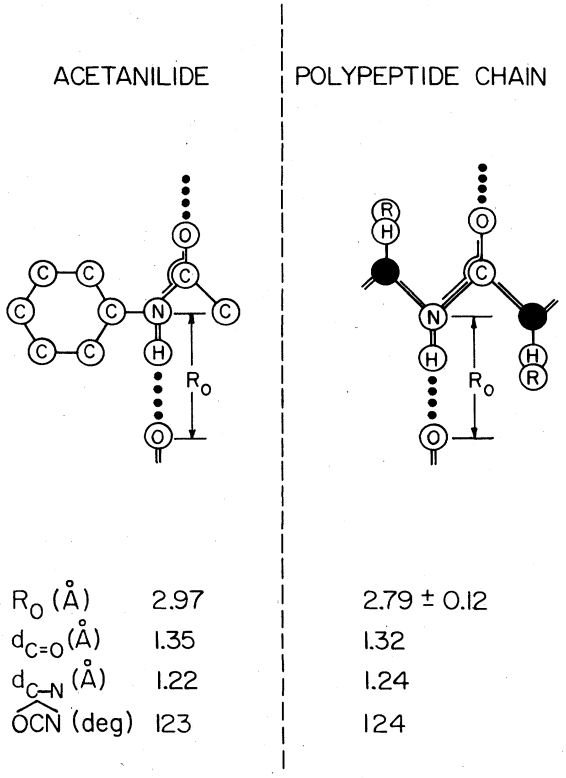

FIG. 1. Comparison of peptide geometry in ACN and in polypeptides.

of self-trapping in condensed matter physics is not new. A half century ago Landau suggested that an electron in a crystal should be self-trapped in the potential well caused by its polarization field.[4] Self-trapping of vibrational quanta was introduced ten years ago by Davydov in the context of α-helix in protein as a means for the storage and transport of biological energy.[5] Since that time Davydov and his co-workers have discussed many aspects of this mechanism[6] and biochemical implications have been described in a recent book.[7] To conform with current usage we shall use the generic term "soliton" for all self-trapped states.[8]

Since this paper is primarily experimental we begin with a discussion of our methods followed by a presentation of our raw experimental results. In the next section we assign the observed bands and show that the above-mentioned 1650-cm^{-1} band has no conventional interpretation. This is followed by a simple version of the soliton theory which contains the main features of the problem but does not treat details of the crystal structure. Finally we discuss the intensity of the soliton line and present conclusions.

II. MATERIALS AND METHODS

A. Materials

Different sources of ACN have been employed including Merck, Test proanalysis, and zone refined 99.99% by Aremco Products, Briarcliff Manor, New York. N^{15} isotropic substitution (95%) was obtained from the Pro-Chem, Rome, Italy, 1977, special product. p-Cl-ACN was from Fluka AG, Hauppauge, New York, purum 99%. The purchased material displays a broad band in the 1700-cm^{-1} region of about 5—10 % of the intensity of the amide I band at 1660 cm^{-1}. p-Cl-ACN was dissolved in trifluoroacetic acid and then recrystallized. This procedure removes the spurious band at 1700 cm^{-1} after crystallization and reproducible results were obtained. NN′ (diacetyl esamethylene diamide) and nylon-6,6 were a gift of the SNAM Progetti Laboratory, San Donato, Italy. Be, Pi (picolinamide), and Ni were obtained from the BDH Lab, England (British Drug House, Ltd.), reagent grade, no less than 98.5% purity. (The symbols for these materials are defined in the caption of Fig. 9.)

Oriented crystals of ACN for ir-absorption measurements were obtained by cooling a thin layer of melted ACN between two Irtran-II windows. The control of the thickness was obtained by applying pressure during cooling. By touching the melted ACN at the edge of the window, large areas of uniform orientation were produced. The normal habit is tabular on 100 and thus the polarized spectrum with the E vector parallel and perpendicular to the b axis was measured.

Samples of polycrystalline ACN were prepared by mixing ACN crystalline powder with ir grade KBr. Pellets of $\frac{1}{2}$-in. diameter were obtained using 10 kbar of pressure.

Amorphous ACN samples were prepared by vacuum deposition on Irtran-II windows of evaporated ACN material. The ACN microcrystals were placed in a small heater with a carefully controlled temperature. At a temperature of about 100 °C the ACN material sublimates under vacuum. The evaporated material was deposited in a form of a homogeneous thin layer on a cool Irtran-II window until the desired optical density was achieved. The spectra of this deposited sample were measured. To achieve annealing of the amorphous sample, low heating was then applied until melting of the thin layer was obtained. Upon cooling, the crystalline properties were recovered. On occasion this annealing procedure was repeated for several cycles.

B. Instrumentation

ir spectra were obtained using three different ir spectrophotometers. For the study of the temperature dependence of the amide I region, a Nicolet (Madison, Wisconsin) model no. 7000 Fourier-transform ir spectrophotometer was used. Spectra were collected for 100 scans using a bandwidth of 0.5 cm^{-1}. The sample was thermostated using a closed-cycle helium refrigerator from Lake Shore Cryotronics, Inc. (Columbus, Ohio), equipped with calcium-fluoride windows. N^{15} and p-Cl-ACN experiments were performed using a Perkin-Elmer model no. 180 grating spectrophotometer equipped with a digital interface. Data were collected at 1-cm^{-1} resolution and stored in a Laben model no. 70 minicomputer for further analysis. Polarized spectra of single crystal and spectra of the series of amide crystal were obtained with a Beckman model no. IR9 spectrophotometer using Beckman gold wire polarizers.

Far-ir-absorption spectra were measured using a Michelson interferometer (model no. 720) equipped with a Golay cell. Samples consist of pellets obtained from a mixture of grounded ACN and polyethylene powder. Pure polyethylene pellets were used to measure background transmission.

Raman spectra were excited by a Coherent Radiation model no. 52 argon ion laser operating at 4880 Å or 5145 Å, with stabilized output power of 20—200 mW. Incident light was filtered by proper choice of interference filters (in order to avoid plasma lines) and its intensity was monitored using a beam-splitter and a silicon photocell. Scattered light was analyzed by a Jarrel-Ash model no. 25-300 Raman spectrometer and detected by an ITT (Fort Wayne, Indiana) model no. FW-130 cooled photomultiplier using photon counting electronics. Spectral resolution was 1 cm^{-1} and wave-number accuracy was ± 2 cm^{-1} from 10 to 3500 cm^{-1}. Samples consist of pellets and small-size crystals of ACN and derivatives and were placed on a copper sample holder at an angle of about 30° from the laser direction (in a reflecting geometry). The holder was located in a modified Cryo-Tip (Waltham, Massachusetts) refrigerator operating down to 20 K. To reduce laser heating on sample surface, a flow of prerefrigerated helium gas was admitted into the sample chamber. The sample-holder temperature was monitored with a platinum resistor placed inside the copper block while actual sample temperature was evaluated from the intensity ratio between Stokes and anti-Stokes Raman lines.

Lattice parameters for powdered ACN have been measured by a conventional vertical Philips (Eindhoven, The Netherlands) x-ray diffractometer equipped with a proportional counter, a copper target, and a nickel filter. The

sample holder, consisting of a small copper plate with a cavity where the powdered sample was pressed, was supported by a cold tip. Fine alignment of the sample holder was performed by using the shadow of the x-ray beam scattered through this cavity, thus reaching an angular accuracy of $\pm 0.01°$. Since 15 relevant reflections (in part overlapping) fall in the small range of 12° to 13°, the computation of the lattice parameters gave a standard deviation of 0.005 Å for a and 0.001 Å for b and c, where a, b, and c are the lattice parameters. After several runs, a more realistic standard deviation has been estimated to be 0.012 Å for a and 0.006 Å for b and c.

To measure the specific heat of crystalline ACN powder, a conventional calorimeter was built. The calorimeter consists of a 20-cm^3 cell made of about 22 g of golden copper, where an Ohmic heater $R1$ and a thermocouple $T1$ were placed. The sample of ACN under He gas was sealed inside the cell using araldite and the cell suspended by nylon wires inside a shielded chamber equipped with an Ohmic heater $R2$. A thermocouple measured the temperature difference ΔT between the cell and the shielding chamber to control the power on heater $R2$ to keep ΔT close to zero. Data were usually taken by heating $R1$ at constant power and measuring the heating rate of the cell, but transient operation also gave quite consistent results. The thermometer $T1$ was a silicon diode (Lake Shore Cryotronics, Inc.), with a temperature coefficient of 2.5 mV/K and an accuracy of 0.6% on C_p in the temperature range 80 to 270 K after proper calibration with a standard thermometer. The measured C_p was independent of heating power in the range 0.10 to 0.40 W, corresponding to heating rates ranging from 0.30 to 1.35 K/min.

III. EXPERIMENTAL RESULTS

A. Thermal expansion

Lattice parameters of powdered crystalline ACN obtained at several temperatures in the range from liquid nitrogen to room temperature are reported in Table I. To facilitate comparison with similar data on other substances reported in literature, the volume of the elementary cell $V=\vec{a}\cdot\vec{b}\times\vec{c}$ is plotted in Fig. 2 as a function of temperature.

B. Specific heat

The specific heat of powdered crystalline ACN has been measured from liquid nitrogen to room temperature.

TABLE I. Lattice parameters of powdered ACN.

T (K)	a (Å)	b (Å)	c (Å)
298	19.623	9.489	7.984
273	19.618	9.481	7.965
223	19.590	9.465	7.927
196	19.568	9.452	7.910
180	19.566	9.445	7.901
158	19.577	9.443	7.888
130	19.545	9.425	7.873
103	19.549	9.425	7.863
87	19.541	9.419	7.865

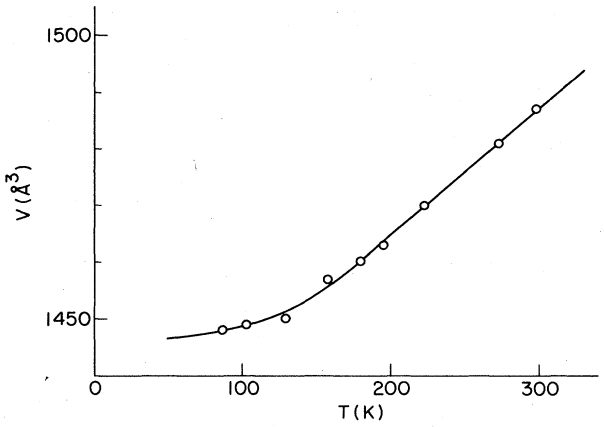

FIG. 2. Volume of the unit cell of ACN crystals as a function of temperature.

Results of three runs obtained with different heating powers W (in units of W) are reported in Table II. Data were fitted using the equation

$$C_p(T)=4.59\times 10^{-3}T+1.505 \quad (3.1)$$

in units of J g^{-1}K^{-1} where T is the temperature measured in °C, to facilitate a comparison with similar data reported in the literature. In Fig. 3 the value of the specific heat as a function of temperature is plotted.

C. ir-absorption spectra

The ir spectrum of microcrystalline ACN from 40 to 4000 cm^{-1} is reported in Fig 4 at 300 and 77 K. At higher frequencies the spectrum is dominated by the amide and phenyl modes. For the 300-K spectrum the major amide vibrations are distinguishable. A major change upon cooling appears in the amide I region where a new band at 1650 cm^{-1} appears. All other bands of the spectrum above 300 cm^{-1} show maximum shifts on the order of 5—10 cm^{-1}, and at low temperature the width is generally decreased. In the low-frequency region below 200 cm^{-1} where phonon modes dominate, there is a general shift toward higher frequencies on cooling and a sharpening of all bands.

A detailed temperature study of the amide I region is

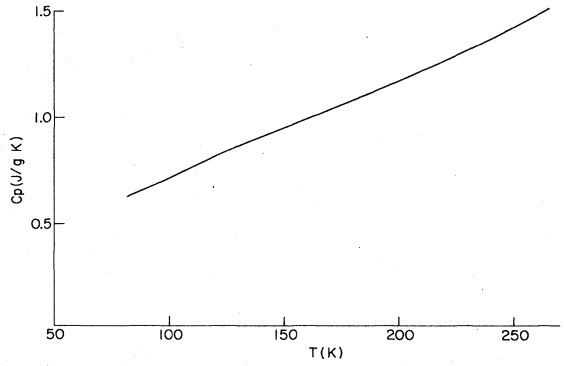

FIG. 3. Temperature dependence of the specific heat of ACN powders.

TABLE II. Specific heat of powdered ACN.

T (K)	C_p (J/Kg) $W=0.10$ (W)	$W=0.25$ (W)	$W=0.45$ (W)
82.53	0.633	0.633	
87.02	0.654	0.654	
91.50	0.675	0.675	
95.98	0.697	0.698	0.698
100.45	0.720	0.720	0.721
104.92	0.743	0.741	0.744
109.37	0.765	0.770	0.768
113.82	0.787	0.787	0.789
118.25	0.810	0.810	0.811
122.68	0.829	0.831	0.830
127.09	0.851	0.852	0.852
131.49	0.868	0.870	0.871
135.87	0.889	0.890	0.891
140.24	0.907	0.911	0.909
144.59	0.926	0.926	0.929
148.93	0.945	0.946	0.947
153.24	0.963	0.966	0.966
157.54	0.982	0.981	0.983
161.82		1.002	1.002
166.07		1.018	1.020
170.30		1.037	1.037
174.51		1.054	1.056
178.70		1.072	1.073
182.86		1.091	1.089
186.99		1.111	1.110
191.09		1.129	1.127
195.17		1.144	1.146
199.22		1.165	1.164
203.24		1.185	1.184
207.22		1.202	1.201
211.18		1.223	
215.10		1.241	
218.98		1.260	
222.83		1.278	
226.65		1.300	
230.43		1.320	
234.17		1.340	
237.87		1.356	
241.53		1.379	
245.14		1.395	
248.72		1.418	
252.25		1.434	
255.74		1.454	
259.19		1.468	
262.58		1.489	
265.94		1.509	

reported in Fig. 5. The intensity of the band at 1650 cm^{-1} increases on cooling without apparent change in frequency and shape. Instead, the amide I absorption at 1667 cm^{-1} decreases in intensity, shifts to higher frequency, and becomes sharper. The peak intensities of the 1650-cm^{-1} band as a function of temperature are reported in Table III.

Polarized ir spectra clearly show that the polarization direction of the band at 1667 cm^{-1} and of the band at 1650 cm^{-1} are the same (Fig. 6). N^{15} isotropic substitution shifts both amide I bands by the same amount (Fig. 7). Other amide bands are also shifted, in particular, the amide II at 1560–1570 cm^{-1}.

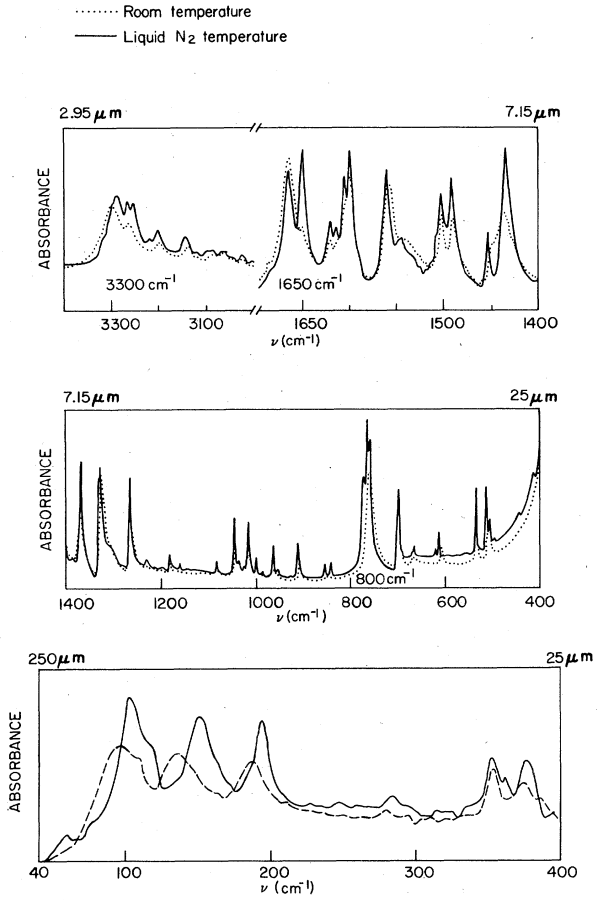

FIG. 4. ir-absorption spectra of ACN. · · · ·, 300-K spectrum; ——, 77-K spectrum.

The band at 1650 cm^{-1} is weak in the amorphous material at 87 K (Fig. 8). Also, the crystal splitting displayed by many of the phenyl-ring frequencies is not present in the amorphous material, as can be seen for the modes at 1600, 1500, and 1420 cm^{-1}. The amide II band is at 1560 cm^{-1} in the amorphous sample. After anneal-

TABLE III. Peak intensity of the 1650-cm^{-1} band.

T (K)	I (arbitrary)
10	158
40	153
60	149
80	140
100	120
120	105
140	90
160	80
180	68
200	53
240	35
280	25
320	15

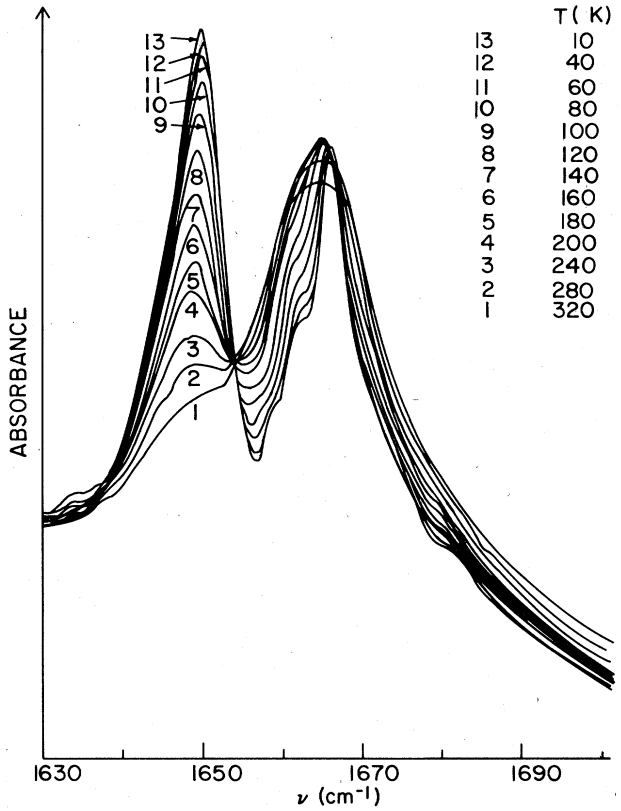

FIG. 5. ir-absorption spectra of ACN microscrystals in KBr in the region of the amide I mode. Results of 100 scans on a Nicolet model no. 7000 FTIR at 0.5 cm^{-1} resolution.

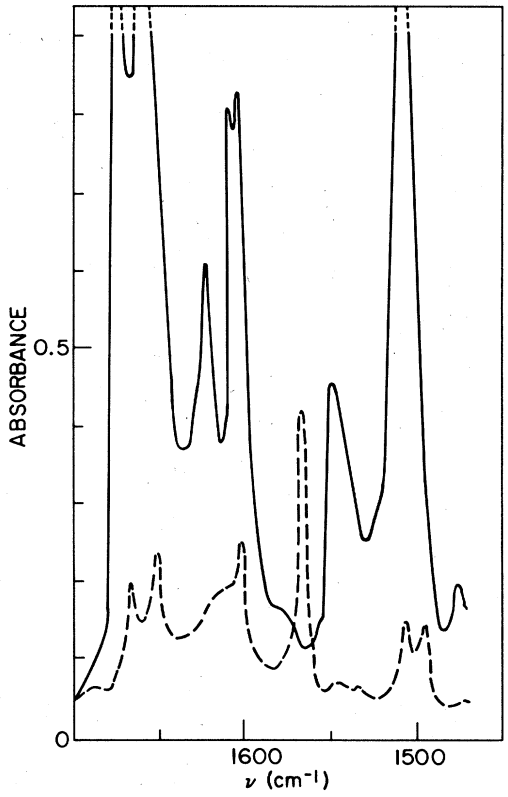

FIG. 6. Polarized ir spectra of ACN crystals. *E* vector parallel to the *b* axis (——). *E* vector perpendicular to the *b* axis (— — —).

ing, most of the crystalline properties are recovered as well as the band at 1650 cm^{-1}.

In a large number of runs, no hysteresis or time relaxation have been observed in the ir intensity over the entire spectrum and for temperature changes from 10 K to room temperature. All spectra taken at the same temperature were coincident within experimental error. Another series of thermal cycles were carried out between 40 and 10 K. Also in these experiments no dependence on the cooling rate or hysteresis was observed.

In view of its intrinsic interest for the properties of the hydrogen bonding we present in Fig. 9 a plot of the N · · · O distance versus their amide I frequency measured by us for a series of related amide molecules. Disregarding the p-Cl-ACN point, the best-fit straight-line equation is

$$d_{N\cdots O}=3.203\times10^{-3}\nu-2.362 \qquad (3.2)$$

in units of Å with ν in units of cm^{-1}. This implies that the change in energy (J) per meter of change in the N · · · O distance is approximately 6.2×10^{-11} N. Details of the ir spectrum of purified p-Cl-ACN in the region 1700—1600 cm^{-1} are given in Fig. 10 and in the NH stretching region are reported in Fig. 11 at room temperature where x-ray data are available.

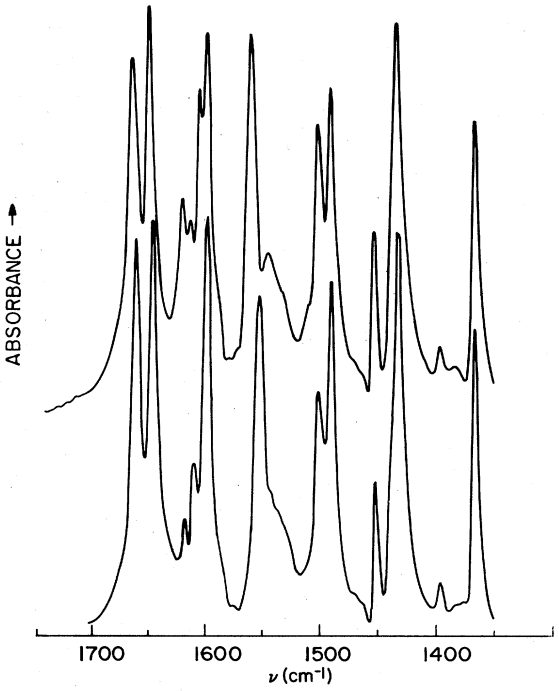

FIG. 7. Upper ir spectrum is normal ACN at 77 K. Lower ir spectrum is N^{15} substituted ACN at 77 K.

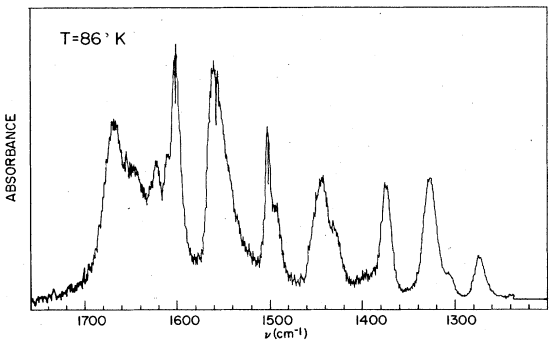

FIG. 8. ir spectrum of amorphous ACN at 86 K.

D. Raman scattering

Raman spectra at 300 and 50 K in the region of the amide modes are reported in Fig. 12. The major changes upon cooling occur in the amide I region where the band at 1650 cm^{-1} increases in intensity at low temperature. A detailed temperature study of this band is reported in Fig. 13. The qualitative behavior is similar to that observed in the ir spectrum of the same band. The Raman spectrum for the low-frequency region from 180 to 20 cm^{-1} for 300 and 50 K of temperature values is reported in Fig. 14. As a general observation, there is an increase of the peak frequencies upon cooling and a narrowing of the bands.

IV. DISCUSSION OF EXPERIMENTAL RESULTS

A. Equilibrium properties

Temperature dependence of specific heat $C_p(T)$ and of volume expansion $V(T)$ are sensitive tests for the presence of a phase transition. Occurrence of a first-order phase transition in crystalline ACN is ruled out because a monotonic temperature dependence is displayed for $C_p(T)$ (Fig. 3) and for $V(T)$ (Fig. 2). At high temperature, the specific heat of ACN increases linearly with temperature with a slope of 0.004 59 J/g, to be compared with 0.003 53 in *o*-chlorobenzoic acid ($C_7H_5ClO_2$) and 0.003 57 in *o*-nitrobenzoic acid ($C_7H_5NO_4$), the two substances with seven carbon atoms where $C_p(T)$ data have been reported.[9] The volume expansion $V(T)$ observed here for ACN is quite close to that reported for urea, a hydrogen-bonded

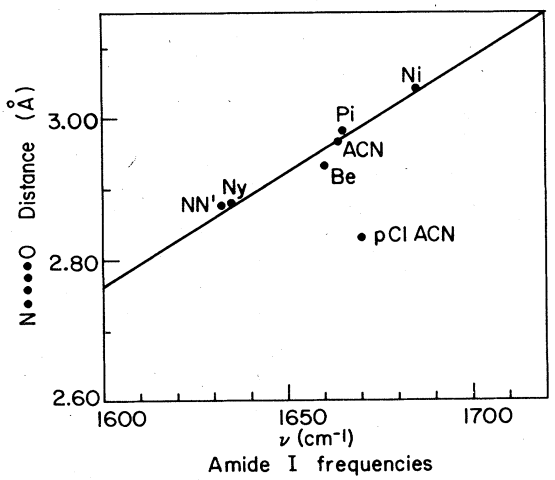

FIG. 9. Dependence of the amide-I frequency on the N · · · O distance in a series of amide crystals. ACN acetanilide, NN' represents N,N' diacetylesamethylendiannime, Ny represents nylon 6.6, Be represents benzamide, Pi represents picolinamide, Ni represents nicotinamide, and p-Cl-ACN represents parachloroacetanilide.

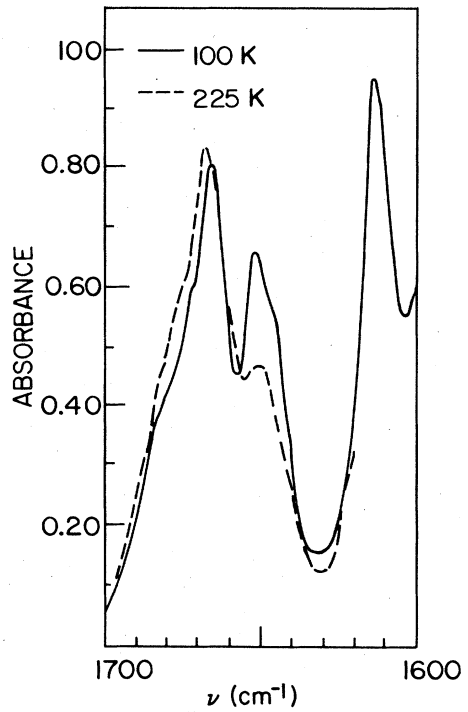

FIG. 10. ir spectrum of p-Cl-ACN at 100 and 225 K in the amide I region.

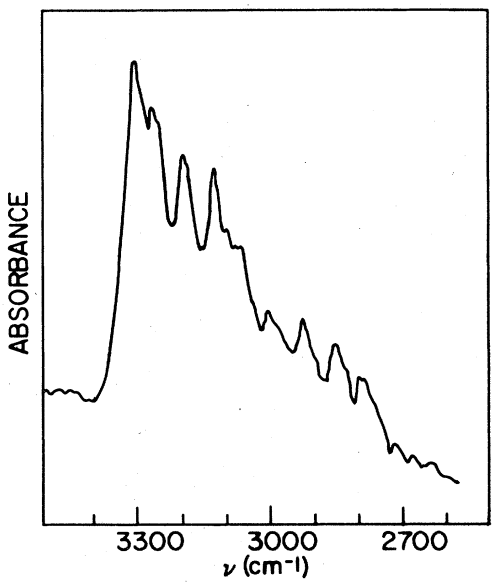

FIG. 11. ir spectrum of p-Cl-ACN at 300 K in the N—H stretching region.

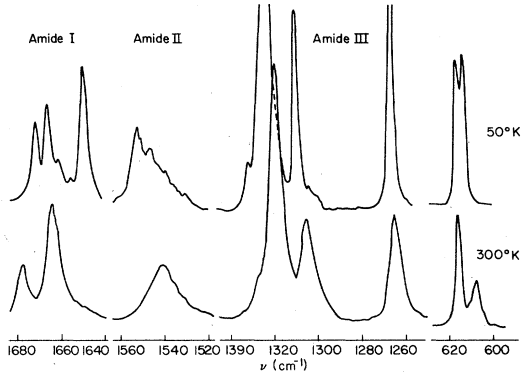

FIG. 12. Raman spectra in the region of the amide modes.

crystal which has been studied by x-ray and neutron-diffraction techniques in the same temperature range,[10] and where no phase transition has been detected.

B. Vibrational modes of ACN crystal

Until now, vibrational spectroscopy of ACN crystal has not received much attention from either the experimental or theoretical viewpoint. Published experimental work refer to ir dichroic absorption of intramolecular vibrations at room temperature[11] and to polarized Raman spectroscopy of low-frequency modes down to 110 K (Ref. 12), while theoretical work is limited to a brief analysis of amide modes in ir.[13] Our work represents the first extensive experimental investigation of ir and Raman vibrational spectra of solid ACN in a wide range of frequency and temperature (10—350 K), including some results on N^{15} isotopic substitution and Cl substitution at the phenyl

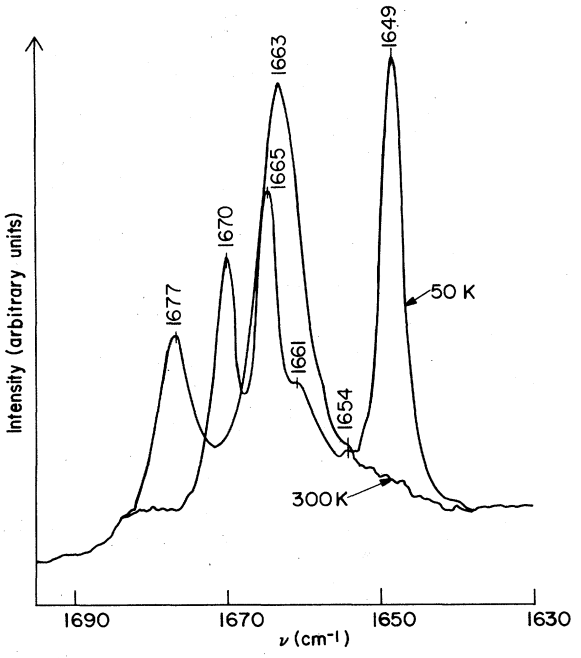

FIG. 13. Raman spectra of the amide I region at 300 and 50 K.

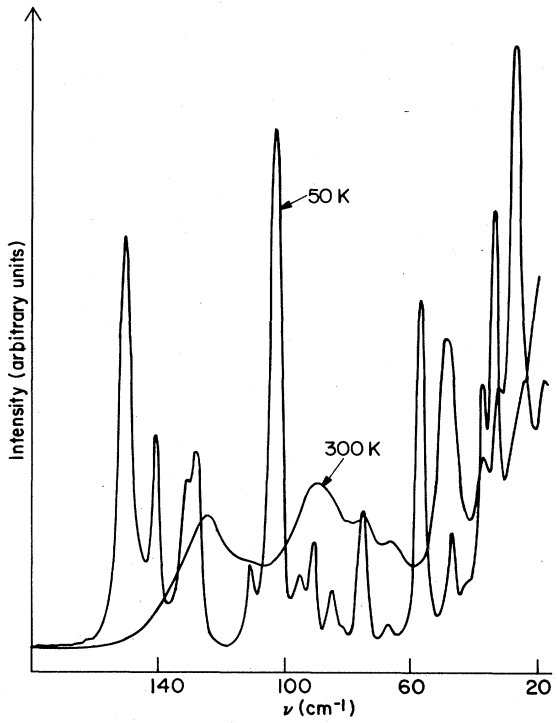

FIG. 14. Raman spectra of the low-frequency modes at 300 and 50 K.

ring. However, owing to the complexity of the single molecule (51 intramolecular vibrations are expected), and due to the large number of molecules per unit cell ($Z=8$) we do not attempt, here, a full assignment of ir and Raman spectra of ACN crystal, but give a qualitative survey of important vibrational modes, i.e., external (phonon) modes and internal modes related to phenyl and amide moities essentially confirming the previous assignments. Only for the amide I vibration, which exhibits a particularly unusual and remarkable behavior as previously reported,[2] a deeper examination is presented.

1. Phonon modes

In ACN crystals, the space group is *Pbca* (D_{2h}^{15}) and the site group is C_1. Vibrational modes are therefore classified according to irreducible representation of the D_{2h} factor group: modes belonging to "gerade" representation are Raman active, *B*-type "ungerade" modes are ir active and Au modes are inactive.[14] Optical external modes at zero wave vector contain 21 translational modes (12 Raman active, 6 ir active, and 3 inactive) and 24 librations (12 Raman active, 9 ir active, and 3 inactive). Room-temperature Raman spectra show a relatively small number of bands at low frequency but, upon cooling, a rich structure appears (Fig. 14). The observed number of peak frequencies is in agreement both with the group-theoretical prediction of 24 Raman-active external modes and with previously published experimental results.[12]

In a detailed study of the phonon region during cooling from room temperature to 35 K, two main effects are observed: the shift of peak frequencies to higher wave num-

bers according to a linear relationship $\nu(T)=\nu(0)-\alpha T$ (where α is in the range 0.01 to 0.1 cm^{-1}/K), typical of anharmonic coupling, and the usual sharpening of bandwidths, which may exceed 20 cm^{-1} at 300 K (for a single mode) and reduces to less than 2 cm^{-1} at 35 K. Moreover, it is noteworthy that all spectral changes induced by temperature in low-frequency vibrations are continuous, confirming the absence of a crystal phase transition, at least in the range 35—350 K, in agreement with x-ray diffraction and specific-heat results.

2. *Internal phenyl modes*

The phenyl ring, possessing 30 internal degrees of freedom, accounts for most of the vibrational features above 200 cm^{-1} in the ir and Raman spectra of ACN. For band assignments we can use accurate vibrational analyses of the benzene ring,[15–17] taking into account the following relevant effects: (i) the linkage with the acetamide group reduces the symmetry from D_{2h} to C_1, shifts vibrational frequencies (up to 50 cm^{-1} or more), and allows ir and Raman vibrational modes which are strongly forbidden in the full D_{2h} symmetry; (ii) the coupling between aromatic rings in the unit cell introduces a further splitting mechanism of intramolecular vibrations (Davydov splitting); and since the strongest interaction is expected for phenyl groups belonging to nearest molecules in different hydrogen-bonded chains, we expect at least a doubling of the phenyl-ring frequencies. These considerations can be applied, for instance, to CC stretching modes in the 1600-cm^{-1} region, which represent a main feature of both ir and Raman spectra. Vibrational bands in this region correspond to the e_{2g} mode of the benzene molecule which appears at 1599 cm^{-1} in the vapor-phase Raman spectrum. Symmetry lowering of phenyl group in ACN makes this mode active also in ir and splits the original vibrational frequency to about 1620 and 1605 cm^{-1}. Each component is further split by the crystal field and typical multiplets appear at low temperature separated by about 5 cm^{-1}. A tentative assignment of some phenyl-group frequencies (CC stretching modes, CH stretching and bending modes, breathing modes, etc.), has been performed and results are shown in Table IV. In all cases, a conclusive test for vibrational assignment has been the insensitivity of vibrational frequencies to isotopic substitutions in the amide moiety.

Temperature dependence of these bands is quite usual: frequency shifts between room temperature and 50 K are within 5 cm^{-1} and bandwidths decrease on cooling by only a few wave numbers (phenyl bands are sharp also at room temperature). Only the doublets in the Raman spectra (at 610—615 cm^{-1} and 1494—1505 cm^{-1}) exhibit some changes (which are of uncertain origin) as temperature decreases.

3. *Amide modes*

Much effort has been devoted to characterization of vibration of the CONH group in model amides and peptides[16–19] and principal associated frequencies are usually classified as follows: (i) amide I, occurring in the range 1630—1680 cm^{-1}, which involves mainly CO stretching and displaces upon deuteration (COND); (ii) amide II, at about 1520—1570 cm^{-1}, corresponding to coupling between NH bending and CN stretching vibrations, which shifts downward (>80 cm^{-1}) upon deuteration and is sensitive to N^{15} substitution; (iii) amide III, around 1300 cm^{-1}, containing a large percentage of NH bending and shifts on deuteration to 900—1000 cm^{-1}; (iv) amide IV to amide VII, at frequencies below 800 cm^{-1}, corresponding to out-of-plane vibrations of the CONH group, sensitive to deuteration and strongly coupled to vibration of nearby groups; (v) amide *A* and amide *B*, in the high-frequency region between 3000 and 3300 cm^{-1}, arising from a Fermi resonance between NH stretching and the amide I overtone and very sensitive to both H and N isotopic substitution. Following these criteria and comparing spectra with different isotopic substitution we made the assignment of amide frequencies in ir and Raman spectra of ACN as shown in Table V. As was previously reported,[2] dramatic

TABLE IV. Room-temperature phenyl-group frequencies in ACN.

$\tilde{\nu}$ (cm^{-1})		Component	Parent benzene mode
1622 1616	ir	CC stretching	vibration no. 8, e_{2g}
1606 1599	ir, Raman		
1503 1492	ir, Raman	CC stretching	vibration no. 13, e_{1u}
1305	Raman	CC stretching	vibration no. 14, b_{2u}
1044 1033	ir, Raman	CH in-plane bending	vibration no. 18, e_{1u}
998	ir (v.w.), Raman	breathing	vibration no. 1, a_{1g}
774 754	ir, Raman	CH out-of-plane bending	vibration no. 11, a_{2u}
615 609	ir (v.w.), Raman	CCC in-plane bending	vibration no. 6, e_{2g}

TABLE V. Room-temperature amide frequencies in ACN.

$\tilde{\nu}$ (cm^{-1})	Tentative assignment
3000–3300 (ir, Raman)	amide *A,B*
1677 (Raman)	amide I
1665 (ir, Raman)	
~1540 (ir, Raman)	amide II
1320 (ir, Raman)	amide III
~620 (ir)	amide IV or VI
~750 (ir)	amide V

temperature effects are observed in the amide I region, which will be analyzed in detail below. Temperature effects are much less relevant in other amide bands, for example, the amide II Raman band (Fig. 12), which is broad (half-width of about 15 cm^{-1}) and symmetrical at room temperature and becomes strongly asymmetrical at low temperature, shifting the peak about 15 cm^{-1} upward but remaining quite broad.

C. Amide I region

1. Tentative assignments of amide I vibrations

At room temperature two principal vibrational frequencies appear in the amide I region: at about 1677 cm^{-1} in the Raman spectrum and around 1665 cm^{-1} in both Raman and ir spectra. From the low-temperature (10 K) ir spectrum in Fig. 5, it is evident that the 1665-cm^{-1} band is composed of three vibations at 1665, 1662, and 1659 cm^{-1}. Since these measurements were made on microcrystalline powder, it is expected that the three ir-active modes (B_{3u}, B_{2u}, and B_{1u}) will have intensities proportional to the components of the amide I transition dipole moment along the three crystal axes (*a*, *b*, and *c* or *x*, *y*, and *z*). From Ref. 11, this moment is oriented in the N—C=O plane about 20° from C=O toward the N—C direction and the corresponding unit vector has components of magnitude 0.303, 0.934, and 0.191 in the *x y*, and *z* directions, respectively. Thus we make the tentative assignments:

Frequency (cm^{-1})	Tentative assignment	Predicted intensity
1665	B_{2u}	0.934
1662	B_{1u}	0.303
1659	B_{3u}	0.191
1650	?	

and note that the predictions of relative intensity are in agreement with Fig. 5. Furthermore, these observed frequency differences between the B_{2u}, B_{3u}, and B_{1u} modes are greater than those calculated in Ref. 13 from dipole-dipole interactions assuming a relative dielectric constant of unity. There is no place for the 1650-cm^{-1} vibration in this assignment scheme.

There are four conventional amide I Raman-active modes in ACN: A_g, B_{1g}, B_{2g}, and B_{3g}. We have estimated the splitting between *A* and *B* modes by calculating the effect of dipole-dipole interactions (as described in Ref. 3) between 16 molecules belonging to two nearby hydrogen-bonded chains in three adjacent unit cells. A Raman-active mode with A_g symmetry is found at a frequency $20.1/\kappa$ cm^{-1} above a mode that is both Raman and ir active (where κ is the effective value of the relative dielectric constant). Furthermore, we note that modes B_{1g}, B_{2g}, and B_{3g} generate components α_{xy}, α_{xz}, and α_{yz}, respectively,[14] in the polarizability tensor defined by

$$\begin{bmatrix} P_x \\ P_y \\ P_z \end{bmatrix} = \begin{bmatrix} \alpha_{xx} & \alpha_{xy} & \alpha_{xz} \\ \alpha_{xy} & \alpha_{yy} & \alpha_{yz} \\ \alpha_{xz} & \alpha_{yz} & \alpha_{zz} \end{bmatrix} \begin{bmatrix} E_x \\ E_y \\ E_z \end{bmatrix} . \tag{4.1}$$

Since (as noted above) the amide I transition dipole moment is oriented primarily in the *y* direction with smaller components in the *z* and *x* directions, we expect to find large differences in the intensities of the three B_g components. Taking into account temperature dependence, we make the following tentative assignment of the lines in Fig. 13.

Temperature (K)	Frequency (cm^{-1})	Tentative assignment
50	1670	A_g
300	1677	
50	1665	
50	1661	B_{1g}, B_{2g}, or B_{3g}
50	1654	
300	1663	$B_{1g}+B_{2g}+B_{3g}$
50	1649	?

All of these tentative assignments must be confirmed by detailed measurements of polarized ir and Raman spectra, but it is clear that there is no conventional assignment available for the 1650-cm^{-1} frequency.

2. 1650-cm^{-1} band

As already reported,[2] the main change observed on cooling in the vibrational spectra of ACN crystalline samples is the growth of a new band at 1650 cm^{-1}. The integrated intensity of this band increases steadily with decreasing temperature from 350 to 4 K, without an appreciable change in peak frequency. Apart from this temperature behavior, the 1650-cm^{-1} band exhibits many similarities with the 1665-cm^{-1} band, which is dominant at room temperature. In particular, we note the following similarities.

(i) The two bands are active in both ir absorption and Raman scattering.

(ii) Polarized Raman experiments in oriented crystal samples (currently being conducted at Los Alamos) show the same polarization behavior for both bands.

(iii) On N^{15} isotopic substitution the frequencies of the 1665- and 1650-cm^{-1} bands shift at 1661 and 1647 cm^{-1}, respectively. The parallel small shift in both vibrations of 3—4 cm^{-1} is in agreement with a small NH bending content and corresponds to the typical amide I mode shift reported in the literature.

(iv) On deuterium substitution of the amide proton, the frequencies of the 1665 and 1650-cm^{-1} bands are both affected. To quantify this effect, a detailed spectral analysis is necessary, and an extensive study of the deuteration effect will be reported later.

3. *Conventional interpretation of the 1650-cm^{-1} band*

The presence and behavior of the 1650-cm^{-1} band does not have a simple interpretation in terms of usual molecular or solid-state effects. To show this, we discuss some possible conventional explanations and the evidence against them.

(i) Despite the behavior on N^{15} and deuterium substitution, the 1650-cm^{-1} band cannot be considered an additional linear vibrational component of amide I because its polarization behavior is not distinct from that at the 1665-cm^{-1} band, as is required by this hypothesis.

(ii) Another effect that might explain the unconventional band in a conventional manner is as follows. The 1650-cm^{-1} frequency might be coincident with a peak in the density of states of amide I vibrations away from zero wave vector spectroscopically activated by the presence of low-temperature defects in the crystal structure. Similar mechanisms have been reported in some organic solids.[20] Although the presence of crystal defects cannot be completely ruled out in ACN, our crystallographic, calorimetric, and spectroscopic results at low frequency do not show the presence of a density of defects as large as required for relaxing wave-vector selection rules. Moreover, the 1650-cm^{-1} band exhibits the same behavior both after repeated temperature cycles and in samples prepared by different methods, and such repeatibility is unlikely to occur when crystal defects play a major role. In particular, it is noteworthy that the 1650-cm^{-1} band appears in low-temperature ir spectra of amorphous ACN prepared by vacuum deposition of sublimated ACN (where many defects are expected) with an intensity much lower than in crystal samples, but its intensity can be fully recovered after annealing treatments which induce crystallization.

(iii) The 1650-cm^{-1} band might also be explained by an intramolecular process (Fermi resonance) arising from anharmonic interaction between the 1665-cm^{-1} mode and a combination mode of the same symmetry and nearly the same frequency. We note that since the 1665-cm^{-1} mode is not totally symmetric, the interacting mode cannot be a first overtone which in D_{2h} symmetry is always totally symmetric. Because of the complexity of the vibrational spectrum of ACN, however, an accidental quasidegeneracy between two frequencies cannot be ruled out, but a strict correlation should be observed between the splitting of the two interacting modes and their ir intensities. In our case, the zero-order intensity of the amide I fundamental can be assumed much stronger than that of the combination mode. Thus, the following approximate relationship should hold at the first perturbative order:

$$\Delta\nu \equiv \Delta\nu_0 \frac{I(1665)+I(1650)}{I(1665)-I(1650)} , \tag{4.2}$$

where $\Delta\nu$ and $\Delta\nu_0$ are first-order and zero-order separations of the two interacting modes and the I's are ir intensities. Since the intensity of the 1650-cm^{-1} band strongly increases at low temperature, one should observe a corresponding increase of the frequency separation. This frequency separation remains nearly constant (within ± 2 cm^{-1}) so the occurrence of a Fermi resonance seems to be excluded.

(iv) A possible explanation of the two amide I components observed in the ir-absorption spectrum could be the existence of two different configurations with different energy. For instance, the hydrogen-bonded proton could be located in two different potential wells. The ground state A would originate the 1650-cm^{-1} band whereas the 1665-cm^{-1} band should be related to the higher-energy state B. Under this hypothesis the intensity ratio of the two bands in thermodynamical equilibrium conditions is given by

$$\frac{I_A}{I_B} = \frac{\mu_A}{\mu_B}\frac{D_A}{D_B}\exp\left[-\frac{E_A-E_B}{kT}\right] , \tag{4.3}$$

where μ, D, and E are the transition moments, the density of states, and the energies of the two configurations, respectively. If we assume $\mu_A=\mu_B$, $D_B=10D_A$, and $(E_B-E_A)/k=360$ K, Eq. (4.3) agrees reasonably well with the experimental result reported in Table III in the temperature range 300 to 100 K, but fails at lower temperature. In particular, at 20 K the predicted value for I_A/I_B is 2 orders of magnitude lower than the experimental one. This failure can be attributed to the presence of a potential wall which at low temperature strongly reduces the transition rate from B to A and thus, on the time scale experimentally accessible, freezes the system in nonequilibrium conditions. We can disregard this hypothesis following the results of the thermal cycles performed using widely different cooling rates.

Of course (4.3) can be used to fit the experimental results if we assume strongly temperature-dependent parameters, but there are no physical reasons for such temperature dependence of the process. In fact (see Fig. 2), the thermal expansion coefficient below 100 K is nearly zero.

D. Related substances

For completeness we consider some molecular crystals related to ACN, in particular, Me-ACN (Me denotes methyl) and p-Cl-ACN, the crystallographic and spectroscopic properties of which are summarized in Table VI. Actually Me-ACN cannot be compared to ACN either for the molecular configuration or for the crystal structure. For instance, while in ACN the angle between the aromatic ring plane and the amide plane is about 18°, in Me-ACN this angle is about 90°. The C=O distance in Me-ACN is 0.044 Å longer than in ACN; no hydrogen-bond network is present in Me-ACN and the crystal cell is considerably smaller than in ACN. Moreover, x-ray diffrac-

TABLE VI. Crystalline and spectroscopic data of ACN related compounds at room temperature.

Symbol		ACN	Me-ACN	p-Cl-ACN
Formula		$C_6H_5NHCOCH_3$	$C_6H_5NCH_3COCH_3$	$ClC_6H_4NHCOCH_3$
Crystal system		orthorhombic	orthorhombic	orthorhombic
Molecules/cell		8	4	4
Lattice	a	19.640	17.151	9.73
parameters	b	9.483	7.328	12.88
(Å)	c	7.979	6.779	6.56
CO distance (Å)		1.219	1.263	1.22
NO distance (Å)		2.97		2.83 x ray 2.99 ir
NH stretching (cm^{-1})		3285		3300
Reference		21	22	23

tion data show a marked anisotropic motion of the methyl group, which suggests the presence of a statistical distribution in methyl-group orientation.[22] From all these dissimilarities, quite different amide I frequencies are expected and are observed but have not been reported here. At room temperature, a doublet structure occurs in the Raman spectra, centered at about 1640 cm^{-1}. On the other hand, at low temperature, no low-frequency component grows up in the amide I region, as is observed in ACN.

p-Cl-ACN is an interesting substance because the molecules are hydrogen bonded as in ACN, although only along single chains and not in double chains as in ACN. In p-Cl-ACN there are two such chains per unit cell, running parallel to the c axis, and the N · · · O distance reported in the literature is lower than ACN. On the other hand, the ir spectrum of the NH stretching mode region (see Fig. 11), which is a very sensitive test for the hydrogen-bonding distance N · · · O, does not show the broad red-shifted band of the strongly hydrogen-bonded systems.[24] Since the reported C=O distances in p-Cl-ACN and in ACN are quite close, one should expect a similar behavior for both substances in the amide I region. This is indeed the case, as shown in Fig. 10, where a temperature-dependent red-shifted band near the amide I is displayed.

V. ELEMENTARY SOLITON THEORY

In this section we present a theoretical framework for interpreting the unconventional band at 1650 cm^{-1} as absorption by a soliton. To this end we focus attention on a single hydrogen-bonded chain running in the b direction of the crystal and consider only nearest-neighbor interactions. Since our purpose is to describe self-trapping of amide I vibrational quanta by interaction with low-frequency vibrations, we start with a semiclassical Hamiltonian operator

$$\hat{H}=\sum_n (\hat{H}^{(n)}_{\rm am}+H^{(n)}_{\rm lf}+\hat{H}^{(n)}_{\rm int}) , \tag{5.1}$$

where the summation index n counts molecules along the hydrogen-bonded chain and

$$\hat{H}^{(n)}_{\rm am}=E_0\hat{B}^{\dagger}_n\hat{B}_n-J(\hat{B}^{\dagger}_{n+1}\hat{B}_n+\hat{B}^{\dagger}_n\hat{B}_{n+1}) , \tag{5.2a}$$

$$H^{(n)}_{\rm lf}=\frac{W}{2}(\omega^{-2}\dot{q}^2_n+q^2_n) , \tag{5.2b}$$

$$\hat{H}^{(n)}_{\rm int}=\chi q_n\hat{B}^{\dagger}_n\hat{B}_n . \tag{5.2c}$$

The first contribution (5.2a) represents the amide I excitation energy in the nth molecule, E_0 being the energy of the uncoupled transition dipole, J being the strength of dipole-dipole interaction between nearest neighbors and $\hat{B}^{\dagger}_n,\hat{B}_n$ creation and annihilation operators, respectively, for the amide I excitation.

The second term (5.2b) represents the energy of the low-frequency vibrations that are responsible for self-trapping. As was noted in Ref. 2, we believe that these vibrations involve the hydrogen-bonding proton but here we avoid a suggestive notation. For analytic convenience we represent all of the low-frequency vibrations by a single classical harmonic oscillator along the coordinate $q_n(t)$ with frequency ω and elastic constant W. A more detailed analysis that represents several low-frequency modes is presented in Ref. 3.

The third term (5.2c) is the interaction energy between an amide I excitation and a low-frequency vibration with a nonlinear coupling constant χ.[25]

The wave function can be written

$$|\psi\rangle=\sum_n a_n(t)\hat{B}^{\dagger}_n|0\rangle , \tag{5.3}$$

where $|0\rangle$ is the amide I vacuum state and the a_n are time-dependent expansion coefficients which must satisfy the normalization condition

$$\sum_n |a_n|^2=1 . \tag{5.4}$$

Applying variation methods to the energy functional $\langle\psi|\hat{H}|\psi\rangle$ (Refs. 3, 5, and 6) we obtain the following dynamic equations for $a_n(t)$ and $q_n(t)$:

$$i\hbar\dot{a}_n=\left[E_0+\frac{W}{2}\sum_i(\omega^{-2}\dot{q}^2_i+q^2_i)+\chi q_n\right]a_n -J(a_{n+1}+a_{n-1}) , \tag{5.5a}$$

$$\omega^{-2}\ddot{q}_n+q_n=-(\chi/W)|a_n|^2 . \tag{5.5b}$$

We focus our attention on solutions of (5.5) for which the low-frequency oscillators are at rest; thus we set

$$\dot{q}_n = 0 \,. \tag{5.6a}$$

Such solutions are not only stationary with respect to the low-frequency classical motion but also with respect to the amide I excitations. Thus from (5.5b),

$$\frac{d}{dt} |a_n| = 0 \,. \tag{5.6b}$$

Under these assumptions the equations of motion reduce to

$$i\hbar\dot{a}_n = \left[E_0 - \frac{\chi^2}{W}|a_n|^2 + \frac{\chi^2}{2W}\sum_i |a_i|^4\right]a_n - J(a_{n+1}+a_{n-1}) \,, \tag{5.7a}$$

$$q_n = -\frac{\chi}{W}|a_n|^2 \,. \tag{5.7b}$$

In the limiting case of a negligibly small coupling constant χ, we have simply,

$$i\hbar\dot{a}_n = E_0 a_n - J(a_{n+1}+a_{n-1}) \,, \tag{5.8a}$$

$$q_n = 0 \,, \tag{5.8b}$$

and only wave solutions ("excitons" or "vibrons") are allowed. In the long-wavelength limit these become

$$a_n = N^{-1/2}\exp[-(i/\hbar)E_{\rm ex}t] \tag{5.9}$$

with

$$E_{\rm ex} = E_0 - 2J \,, \tag{5.10}$$

where N is the number of molecules in the chain.

In the general case ($\chi \neq 0$) we have both wavelike and localized (self-trapped) solutions. Wave solutions are practically identical to the pure excitonic solutions given by (5.9) and (5.10) because $|a_n|^2 \to 0$ as $N \to \infty$.

Self-trapped solutions (i.e., *solitons)* can be obtained using the general methods discussed in Refs. 3 and 6 which show that we are mainly interested in strongly localized solutions. Thus we assume for simplicity

$$|a_n| \doteq \delta_{n,m} \tag{5.11}$$

to describe a soliton that is strongly self-trapped at site m. Equation (5.7a) then gives

$$i\hbar\dot{a}_m \doteq (E_0 - \chi^2/2W)a_m \tag{5.12}$$

from which

$$a_m = \exp[-(i/\hbar)E_{\rm sol}t] \tag{5.13}$$

with

$$E_{\rm sol} = E_0 - \chi^2/2W \,. \tag{5.14}$$

The energy shift between a fully delocalized exciton (5.10) and a strongly localized soliton (5.14) is therefore

$$\Delta E = E_{\rm ex} - E_{\rm sol} = \frac{\chi^2}{2W} - 2J \,. \tag{5.15}$$

In our case the experimental shift between conventional and unconventional amide I bands gives $\Delta E \doteq 15$ cm^{-1}. The value of J is in the range 1.5–4 cm^{-1} depending on the assumed effective dielectric constant.[3] Thus from (5.15) we obtain

$$\frac{\chi^2}{W} = 36\text{–}47 \text{ cm}^{-1} \,. \tag{5.16}$$

To check that this value is of acceptable order of magnitude, we assume χ to be the value 6.2×10^{-11} N obtained from (3.2). This implies $W = 4.8$ N/m which is reasonable for a force constant related to hydrogen bonding.[27]

At this point the reader might be tempted to raise the following objection to a soliton interpretation for the 1650-cm^{-1} line in Fig. 5. A soliton is generally considered to be a long-lived phenomenon, yet the width of the 1650-cm^{-1} line is of the same order of magnitude as that of the conventional 1665-cm^{-1} line. Thus the lifetime should be about the same for both excitations.

To answer this objection we note that the above analysis has, for clarity of presentation, neglected interaction of localized amide I vibrational energy with acoustic phonons which was the basis for Davydov's original theory.[5–7] This approximation is appropriate on a time scale that is short compared with the time

$$\tau = (M/w)^{1/2} \,, \tag{5.17}$$

where M is the mass of an ACN molecule and w is the spring constant of a hydrogen bond [13 N/m (Ref. 27)]. Thus $\tau = 0.12$ ps which can be interpreted as the time required for an acoustic phonon to propagate from one molecule to the next. From numerical studies of initiation of Davydov's intermolecular soliton,[28] the width of the soliton times τ is the time required to "dig its nest" of nearest-neighbor lattice distortions.

Thus we expect that a significant contribution to the width of the 1650-cm^{-1} line arises from relaxation of the soliton described here into a true Davydov soliton which is self-trapped by acoustic-model vibrations.

VI. INTENSITY OF THE SOLITON LINE

Davydov has shown that the ratio of absorption cross section of an isolated amide I vibration to that of an exciton is equal to b/λ where b is the distance between molecules and λ is the wavelength of incident radiation.[7] Since the number of ir-active excitons per unit distance in the beam direction is b/λ times the corresponding number of amide I vibrations, the total absorption from a beam is the same whether one considers it to be caused by excitons or by individual amide I bands.[2] Therefore the intensity of the soliton line relative to that of the exciton line should depend primarily on the inner product of the ground-state wave function for the low-frequency vibration before soliton absorption to that after absorption.

Thus we return to (5.5b) and note that before soliton absorption, the ground state of the low-frequency vibration is

$$\phi_0 = \left[\frac{W}{\pi\hbar\omega}\right]^{1/2}\exp\left[-q^2\frac{W}{2\hbar\omega}\right] \tag{6.1}$$

and after the soliton transition it is

$$\tilde{\phi}_0=\left[\frac{W}{\pi\hbar\omega}\right]^{1/2}\exp\left[-\left[q+\frac{|a|^2\chi}{W}\right]^2\frac{W}{2\hbar\omega}\right], \quad (6.2)$$

where the subscripts on q and a have been dropped for typographical convenience. The transition probability for soliton absorption is therefore reduced by the Franck-Condon factor

$$\left[\int\phi_0\tilde{\phi}_0 dq\right]^2=\exp\left[-\frac{\chi^2|a|^4}{2W\hbar\omega}\right]. \quad (6.3)$$

Assuming $|a|^2\doteq 1$, the Franck-Condon factor is close to unity for

$$\chi^2/W\ll\hbar\omega \quad (6.4)$$

and close to zero for

$$\chi^2/W\gg\hbar\omega\ . \quad (6.5)$$

For self-trapping by acoustic-mode vibrations, inequality (6.5) is satisfied and as Davydov has emphasized,[7] direct absorption is forbidden.

The frequency ω of the low-frequency mode in (5.5b) can be estimated by noting that the probability of being in the ground state depends upon temperature as $[1-\exp(-\hbar\omega/kT)]^{1/2}$. Thus the intensity of the soliton absorption line is

$$I(T)\propto\exp\left[-\frac{\chi^2|a|^4}{2W\hbar\omega}\right][1-\exp(-\hbar\omega/kT)]^2\ . \quad (6.6)$$

A least-squares fit (see Fig. 15) of the intensity versus temperature data from Table III to the function $I(T)=158[1-\exp(-\hbar\omega/kT)]^2$ requires that

$$\nu\equiv\omega/2\pi c=131\ \text{cm}^{-1}\ . \quad (6.7)$$

From (5.16) and (6.4) the corresponding Franck-Condon factor is close to unity.

Inspection of Fig. 15 shows that the agreement between (6.6) and the data of Table III can be improved if ω is assumed to be a decreasing function of temperature. Since this is suggested from Fig. 14 and measurements by Gerasimov,[12] we are encouraged to solve (6.6) for

$$\nu(T)=\frac{kT}{hc}\ln\frac{1}{1-(I/I_0)^{1/2}} \quad (6.8)$$

in units of cm^{-1}. In Fig. 16 we present calculated values of $\nu(T)$ from the data in Table III. The error bars in this figure are obtained by noting that

$$\frac{d\nu}{dI}=\frac{kT/2hcI_0}{(I/I_0)^{1/2}[1-(I/I_0)^{1/2}]} \quad (6.9)$$

and assuming that the error in determining I is $\pm 0.05\ I_0$. In the temperature range between 100 and 200 K,

$$\nu(T)\doteq 149-0.077T\ , \quad (6.10)$$

in units of cm^{-1} which is in qualitative agreement with results reported in Ref. 12 and in Fig. 14.

For $T<100$ K our measurements of $\nu(T)$ are obscured by error. For $T>200$ K, errors again become important but $\nu(T)$ appears to be falling faster than is indicated in (6.10). This may be an artifact associated with incorrect subtraction of the base line in constructing Table III or a real phenomenon associated with temperature-dependent effects not included in the derivation of (6.6).

One source of additional temperature-dependent effects might be the interaction of the soliton with thermally excited acoustic phonons which has been considered in detail by Davydov.[29] He shows that this interaction leads to a decrease in self-trapping as the temperature is increased. Since thermally excited acoustic phonons act on the soliton by reducing the dipole-dipole—interaction energies, this effect is expected to be small when the solitons are localized near a single amide I vibration as in the present case.

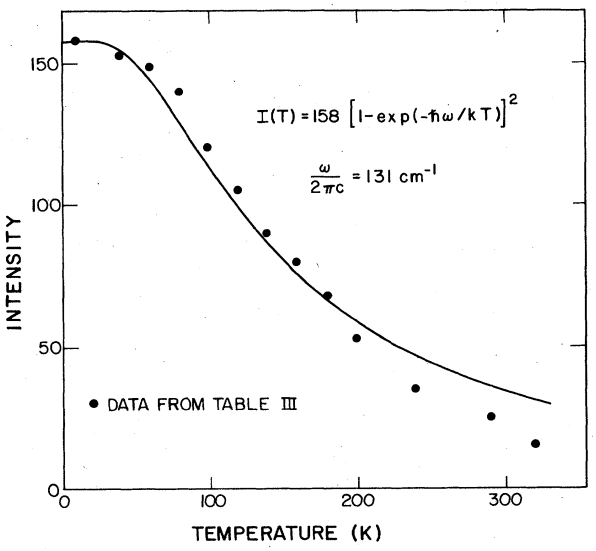

FIG. 15. Least-squares fit of the peak intensity vs temperature data of the 1650-cm^{-1} line (from Table III) to the function $I(T)=158[1-\exp(-\hbar\omega/\kappa T)]^2$.

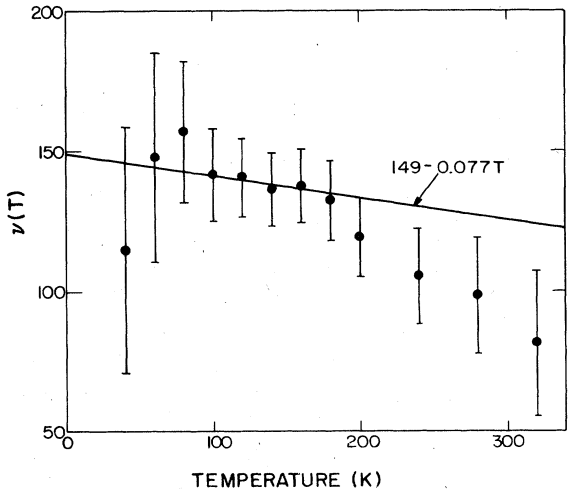

FIG. 16. Calculated values of $\nu(T)=\omega/2\pi c$ from (6.8) and Table III.

VII. CONCLUSIONS

From the above discussion we draw the following conclusions.

(i) The unconventional amide I absorption described in Sec. III is a well-established experimental fact.

(ii) As discussed in Sec. IV, conventional concepts in molecular spectroscopy offer no acceptable explanation for the unconventional amide I band.

(iii) The soliton hypothesis sketched in Secs. V and VI provides a straightforward explanation for both the red shift and the intensity of the 1650-cm^{-1} band.

Thus we suggest that the soliton described here is a new member of the growing family of self-trapped states that have been detected in condensed matter and the first example in an organic solid which is a suitable model for proteins. Perhaps the most important finding of our work is that a soliton on a network of hydrogen-bonded amides can be created by infrared light. Although we are aware of the biological relevance of a light-sensitive soliton, we choose not to discuss those aspects in this paper because they are more appropriate for biochemical journals.

ACKNOWLEDGMENTS

It is a pleasure to express our appreciation to M. Garozzo, G. Grillo, and E. Scafé for experimental assistance in the early stages of this work and to M. Cesari for x-ray measurements at ENI Laboratory. We also thank I. Bigio, C. Johnston, R. Ryan, and B. Swanson for recent discussions of the experimental work and J. C. Eilbeck and P. Lomdahl for contributions to the theory. Special thanks go to S. Califano for illuminating discussions on the molecular spectroscopy aspects of this problem. This work was supported in part by grants from the National Science Foundation (No. PCM 9209616), and from the Department of Health, Education and Welfare (No. HEWPHSGM18051).

[1]G. Careri, in *Cooperative Phenomena,* edited by H. Haken and M. Wagner (Springer, Berlin, 1973), p. 391.

[2]G. Careri, U. Buontempo, F. Carta, E. Gratton, and A. C. Scott, Phys. Rev. Lett. **51**, 304 (1983).

[3]J. C. Eilbeck, P. S. Lomdahl, and A. C. Scott, following paper, Phys. Rev. B **30**, 4703 (1984).

[4]L. Landau, Phys. Z. Sowjetunion **3**, 664 (1933).

[5]A. S. Davydov and N. I. Kislukha, Phys. Status Solidi B **59**, 465 (1973); A. S. Davydov, J. Theor. Biol. **38**, 559 (1973).

[6]See A. S. Davydov, Phys. Scr. **20**, 387 (1979) for a summary of results and bibliography.

[7]A. S. Davydov, *Biology and Quantum Mechanics* (Pergamon, New York, 1982).

[8]A. C. Scott, F. Y. F. Chu, and D. W. McLaughlin, Proc. IEEE **61**, 1443 (1973); R. K. Dodd, J. C. Eilbeck, J. D. Gibbon, and H. C. Morris, *Solitons and Nonlinear Wave Equations* (Academic, London, 1982).

[9]*International Critical Tables* (McGraw-Hill, New York, 1933), Vol. 2.

[10]N. Sklar, M. E. Senko, and B. Post, Acta Crystallogr. **14**, 716 (1961).

[11]N. B. Abbott and A. Elliott, Proc. R. Soc. London, Ser. A **234**, 247 (1956).

[12]V. P. Gerasimov, Opt. Spektrosk. **43**, 705 (1977) [Opt. Spectros. (USSR) **43**, 417 (1978)].

[13]Y. N. Chirgadze and N. A. Nevskaya, Biopolymers **15**, 607 (1976); Dokl. Akad. Nauk SSSR **208**, 447 (1973).

[14]D. L. Rousseau, R. P. Bauman, and S. P. S. Porto, J. Raman Spectrosc. **10**, 253 (1981).

[15]G. Varsanyi, *Vibrational Spectra of Benzene Derivatives* (Academic, New York, 1963).

[16]L. J. Bellamy, *The Infrared Spectra of Complex Molecules* (Chapman and Hall, London, 1975), 3rd. ed. See pp. 72—106 for aromatic compounds and pp. 231—262 for amides.

[17]F. R. Dollish, W. G. Fateley, and F. F. Bentley, *Characteristic Raman Frequencies of Organic Compounds* (Wiley, New York, 1974). See pp. 162—180 for aromatic compounds and pp. 121—133 for amides.

[18]L. J. Bellamy, *Advances in Infrared Group Frequencies* (Methuen, London, 1968), pp. 177—180 and 241—288.

[19]T. Miyazawa and E. R. Blout, J. Am. Chem. Soc. **83**, 712 (1961).

[20]R. J. Nemanich and S. A. Solin, Phys. Rev. B **20**, 392 (1979).

[21]C. J. Brown and D. E. C. Corbridge, Acta. Crystallogr. **7**, 711 (1959); C. J. Brown, *ibid.* **21**, 442 (1966).

[22]B. F. Pedersen, Acta. Chem. Scand. **21**, 1415 (1967).

[23]E. Subramanian, Z. Kristallogr., Kristallgeom., Kristallphys., Kristallchem. **123**, 222 (1966).

[24]N. Sheppard, in *Hydrogen Bonding,* edited by D. Hadzi (Pergamon, London, 1959), p. 85.

[25]A. S. Davydov, *Theory of Molecular Excitons* (Plenum, New York, 1971).

[26]A. C. Scott and L. MacNeil, Phys. Lett. **98A**, 87 (1983).

[27]K. Itoh and T. Shimanouchi, J. Mol. Spectrosc. **42**, 86 (1972).

[28]A. C. Scott, Phys. Rev. A **26**, 578 (1982); **27**, 2767 (1983).

[29]A. S. Davydov, Zh. Eksp. Teor. Fiz. **78**, 789 (1980) [Sov. Phys.—JETP **51(2)**, 397 (1980). See also M. Satarić, G. Vujicić, and R. Zakula, Nuovo Cimento **63B**, 709 (1981).